ELSEVIER

Journal of Luminescence 69 (1996) 85–94

JOURNAL OF LUMINESCENCE

Ce:LiSrAlF$_6$ laser performance with antisolarant pump beam

A.J. Bayramian[a], C.D. Marshall[a,*], J.H. Wu[a], J.A. Speth[a], S.A. Payne[a], G.J. Quarles[b], V.K. Castillo[b]

[a] *University of California, Lawrence Livermore National Laboratory, P.O. Box 5508, Livermore, CA 94550, USA*

[b] *Lightning Optical Corporation, 431 E. Spruce Street, Tarpon Springs, FL 34689, USA*

Received 31 March 1996

Abstract

We have explored the impact of 266 nm pump-induced solarization on the 290 nm laser performance of Ce:LiSrAlF$_6$ crystals. Among the issues considered are the incorporation of codopants (e.g. Na^+, Mg^{2+}, Zn^{2+}), and the use of an additional 532 nm beam to rapidly destroy the interfering color centers. The solarization mechanism has been unraveled and found to involve two-photon creation of color centers (via the 4f → 5d → conduction band pathway of Ce^{3+}), followed by the one-photon bleaching of the color centers. Ce:LiSrAlF$_6$ (Ce:LiSAF) laser slope efficiencies as high as 47% can be achieved with the simultaneous introduction of the 266 nm pump and 532 nm bleaching beams; 33% with the 266 nm beam only.

Keywords: Ce:LiSrAlF$_6$ crystals; Pump beam; Laser performance

1. Introduction

Attempts to identify and devise solid state lasers based on the Ce^{3+} dopant date back almost two decades now, when its potential for laser action based on the ultraviolet (UV) 5d → 4f transition was first explored [1]. The essential physics of the Ce^{3+} ion appears promising for laser action, in that the 5d → 4f transition is strongly dipole-allowed (assuring high gain with a nanosecond-scale pump pulse), and exhibits substantial emission bandwidth for broad tunability [2]. The implementation of Ce-laser technology has been challenged however, by issues surrounding solarization or coloring of the materials, arising from liberating an electron from Ce^{3+} to form color centers [3]. Since color center absorptions are characterized by oscillator strengths an order of magnitude greater than those of 5d–4f transitions ($f = 0.1$–1.0 versus $f = 0.01$–0.1), they can be anticipated to be detrimental to efficient laser performance.

The initial laser demonstrations of crystals such as Ce:LiYF$_4$ and Ce:LaF$_3$ were both enticing and disappointing [1, 3]. While clear observations of laser action were realized [4], UV-induced solarization effects led to low efficiency and repetition rate. Furthermore, as it turns out, other crystals considered such as Ce:CaF$_2$, were afflicted so severely by solarization that it was not possible to achieve lasing [5]. Recent reports of stable laser performance or gain in Ce:LiSrAlF$_6$ [6], Ce:LiCaAlF$_6$ [7], and Ce:LiLuF$_4$ [8] have renewed enthusiasm for the prospects of tunable UV solid state laser sources. These reports must be

* Corresponding address.

PII S0022-2313(96)00081-6

tempered by the general finding that Ce^{3+}-doped materials tend to exhibit UV pump-induced color centers; the color center absorption spectra have been documented for CaF_2 [4, 5], $LiYF_4$ [9], $LiLuF_4$ [10], $LiSrAlF_6$ [6], and $Y_3Al_5O_{12}$ [11].

It is worthwhile to briefly review the basic physics of the UV pump-induced losses impacting the 5d–4f laser transitions. In order for an electron released from the Ce^{3+} ion to then become trapped at a color center, the rare earth ion must first experience an electronic transition from the 5d orbital to the conduction band (CB) of the host medium. Recent articles by Lawson et al. [12] offer extensive characterization of the $5d \rightarrow CB$ transition for the Eu^{2+} rare earth ion in fluorite-structure crystals (e.g. CaF_2, $SrCl_2$, etc.). The $5d \rightarrow CB$ transition is found to be both broad ($\sim$eV) and strong ($f = 0.1$). The spectral width arises from the broad density of states function characterizing the conduction band. Interestingly, the $5d \rightarrow CB$ transition of Eu^{2+} in $LiCaAlF_6$ was also explored and found to be significantly blue-shifted compared to CaF_2 ($\sim$1.5eV). This result is interpreted in terms of the position of the rare earth 5d state being deeper within the band gap, and is strongly suggestive that the favorable laser performance of Ce-doped $LiCaAlF_6$ is traceable to this same phenomenon. The $5d \rightarrow CB$ transition turns out to be weaker and blue-shifted in $LiCaAlF_6$ at the pump and laser wavelengths compared to other Ce-doped crystals, leading to reduced excited state absorption and solarization losses. Fig. 1 qualitatively depicts the relationship between the 4f and 5d levels of Ce^{3+}, the valence and conduction bands of the host, and the existence of trap states (i.e. color centers). It is noteworthy that the case for ascribing the excited state absorption to the $5d \rightarrow CB$ transitions was first made for $Ce^{3+}:Y_3Al_5O_{12}$ [11, 13, 14] on the basis of the theory of Pedrini et al. [15].

The present work builds on several recent papers, including the discovery of Ce:$LiCaAlF_6$ by Dubinskii et al. [7], our own report on Ce:Li $SrAlF_6$ [6], and a parallel effort by Pinto et al. [16] While the $LiCaAlF_6$ and $LiSrAlF_6$ crystals were originally developed as hosts for the chromium ion (viz. Cr:LiSAF), the special utility of Ce^{3+} substituting for Sr^{2+} represents a remarkable extension

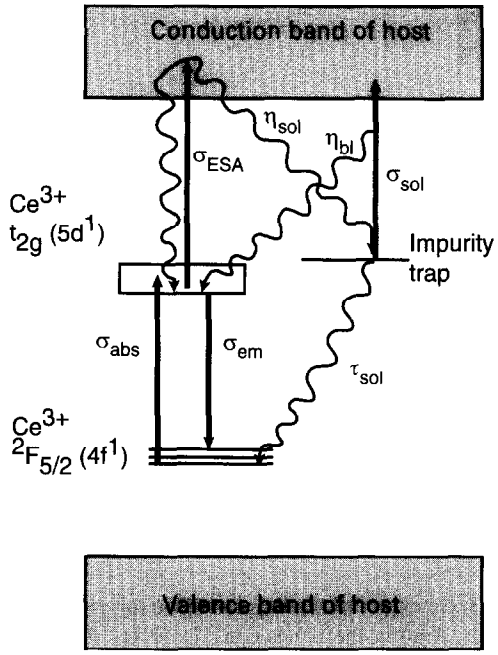

Fig. 1. Qualitative drawing of host band states and Ce^{3+} energy levels suggesting numerous processes that may be important, including Ce ground state absorption (σ_{abs}), excited state absorption (ESA) from Ce^{3+} to the conduction band (CB), color center absorption (σ_{sol}), emission (σ_{em}), and the efficiencies of bleaching and solarization (η_{bl} and η_{sol}).

of utility for this material [17]. Ce:LiSAF nevertheless does benefit from the mature level of crystal growth procedures developed for Cr:LiSAF and the ready availability of high quality material [18]. In fact, Ce:LiSAF has already served as the gain medium in a SO_2 and O_3 lidar system [19].

The content of this article is divided into three main sections: first we document the presence of substantial solarization losses, then the physics of solarization is elucidated, and finally the use of an additional visible pump beam for reduced solarization (and enhanced laser efficiency) is presented.

2. Laser efficiency and pump-induced loss

The absorption and emission spectra of Ce:LiSAF are displayed in Fig. 2 on an absolute cross section scale, as adapted from Ref. [6]. As previously recognized, Ce:LiSAF has been found to operate most efficiently when both pumped and

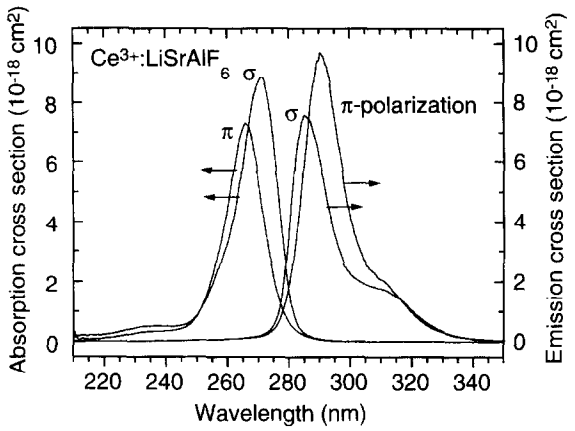

Fig. 2. Absorption and emission spectra of Ce : LiSAF presented on absolute cross-section scales.

lased with the light field π-polarized (i.e. electric field along the c axis of the uniaxial LiSAF host medium). In our previous study we also found that excited state absorption (ESA) at the pump and laser wavelengths has a profound impact on the performance of the laser system. For example, the π-and σ-polarized pump absorption cross-sections (in units of 10^{-18} cm^2) are nearly isotropic at 7.3 and 6.6 at 266 nm, respectively, while the ESA values are 6.5 and 23 – giving rise to an overwhelming preference for π-polarized pumping to avert ESA losses. Similarly, the π- and σ-polarized emission cross-sections at 290 nm are $\sigma_{em} = 9.5$ and 6.1, versus $\sigma_{ESA} = 2.7$ and 4.6 for ESA, respectively. Since the stimulated emission gain cross-sections are given by the difference $\sigma_{gain} = \sigma_{em} - \sigma_{ESA}$, the π- and σ-polarized values are 6.8 and 1.5, respectively, again indicative of a rather large level of gain anisotropy. Table 1 contains a summary of these parameters, and others to be addressed later in this paper. The emission lifetime of Ce : LiSAF was previously measured to be 28 ns.

The slope efficiency obtained with a simple two-mirror, near-confocal Ce : LiSAF oscillator pumped at 266 nm with a quadrupled Nd : YAG laser can be described with [20]:

$$\eta_l = \left(\frac{h\nu_l}{h\nu_p}\right)\eta_p\left(\frac{\sigma_{em} - \sigma_{ESA}}{\sigma_{em}}\right) \times\left[\frac{\ln(1 - T_{oc})}{\ln(1 - T_{oc}) + \ln(1 - L_d)}\right] \quad (1)$$

Table 1
Parameters characterizing Ce : LiSAF laser performance (cross-sections, σ, in 10^{-18} cm^2; efficiencies, η, are unitless)

Parameter/ wavelength	π-polarized	σ-polarized	Source
σ_{abs}/266 nm	7.3	6.6	Ref. [6]
σ_{em}/290 nm	9.5	6.1	Ref. [6]
σ_{ESA}/266 nm	6.5	23	Ref. [6]
σ_{ESA}/290 nm	2.7	4.6	Ref. [6]
σ_{gain}/290 nm	6.8	1.5	Ref. [6]
σ_{sol}/266 nm	–	6.2	Fig. 8
σ_{sol}/457 nm	3.0	13.6	Figs. 5 and 8
η_{sol}/266 nm	–	0.039	Fig. 8
η_{bl}/266 nm	–	(1.0)	Fig. 8; values of 0.3 1.0 acceptable
η_{bl}/457 nm	–	0.046	Fig. 7 with $\eta_{bl}\sigma_{sol}$/ 457 nm

where $h\nu_p$ and $h\nu_l$ are the pump and laser photon energies, η_p is the pumping efficiency, T_{oc} is the output coupling, L_d is the double-pass loss, and the cross-sections correspond to the 290 nm laser output wavelength. η_l is intended to be defined with respect to the absorbed pump energy. If we suggest that η_p can approach unity with appropriate adjustment of the Ce doping density and the pump spot size, then the so-called intrinsic efficiency (i.e. $L_d = 0$; $\eta_p = 1$) is defined as [20]:

$$\eta_0 = \left(\frac{h\nu_l}{h\nu_p}\right)\left(\frac{\sigma_{em} - \sigma_{ESA}}{\sigma_{em}}\right). \quad (2)$$

Substituting in the parameter values yields a theoretical value of $\eta_0 = 66\%$. The experimentally derived value of η_0 is discussed next.

The laser efficiencies of two representative crystals were evaluated with output couplings of 50% and 5%. The Ce : LiSAF crystals were located at the center of a cavity formed by two 10 cm radius-of-curvature mirrors separated by 11 cm. The highest efficiencies (plotted in Fig. 3) obtained for the two output couplers were 33.1% and 5.5% for $T_{oc} = 50\%$ and 5%, respectively. Applying Eq. (1) (with $\eta_p = 1$) we deduced that $L_d = 36\%$ and $\eta_0 = 55\%$. An independent evaluation of a second crystal yielded $L_d = 46\%$ and $\eta_0 = 54\%$. Recalling that the calculated value of η_0 from Eq. (2) above is 66%, we can infer that the remaining discrepancy

can be attributed to the pumping efficiency of $\eta_p = 83\%$.

Overall, the intrinsic efficiency η_0 is understandable in terms of the quantum defect, and ESA at the pump and laser wavelengths. On the other hand, the surprising result is that the single-pass loss of the best samples is in the range of 20%, an enormous value for a sample < 1 cm in thickness. Since we cannot account for this level based on the passive losses present in the material from absorption and scatter ($< 0.2\%\ cm^{-1}$ for LiSAF, $3\%\ cm^{-1}$ for LiCAF), we surmise that pump-induced solarization is responsible for the high loss level. In the next section we explore the basic physics of the solarization mechanism and infer the means by which its adverse impact can be mitigated.

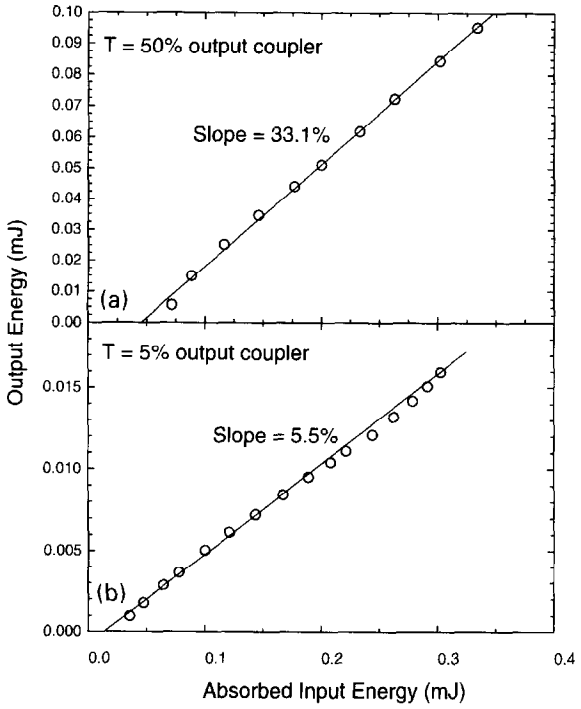

Fig. 3. Laser efficiencies obtained for Ce:LiSAF with 2% Na codoping (in melt) for 5% and 50% output coupling values at 290 nm.

3. Solarization and bleaching

The solarization spectra and its UV pump-induced strength may be influenced by the preparation and composition of the Ce:LiSAF material, including the addition of codopants along with cerium. Since on the basis of ionic size considerations it is only possible for Ce^{3+} to substitute for the Sr^{2+} host ion, the $^{+}1$ charge mismatch can potentially be compensated by the incorporation of additional dopants. The samples tested are listed in Table 2, where it is seen that the Na^+, Mg^{2+}, and Zn^{2+} codopants were considered [21]. The Na^+ codopants are of interest because they can substitute for the Sr^{2+} host sites to provide charge compensation. While the emission spectra of pure Ce:LiSAF and Na-codoped material were similar,

Table 2
Absorption properties and cerium concentrations of laser crystals

Crystal designation[a]	Peak absorption coefficient π—pol (cm^{-1})	Ce^{3+} content from from σ_{abs} ($10^{19}\ cm^{-3}$)	Distribution coefficient
1.5% Ce:LiSAF	10.1	0.140	0.011
2% Ce:LiSAF	17.4	0.242	0.014
2% Na, 2% Ce:LiSAF	15.0	0.208	0.012
4% Na, 2% Ce:LiSAF	12.9	0.179	0.010
2% Mg, 2% Ce:LiSAF	7.8	0.108	0.006
2% Zn, 2% Ce:LiSAF	8.6	0.119	0.007
2% Ce:LiCAF	7.0	0.097	0.006
2% Ce:Li($Sr_{0.8}Ca_{0.2}AlF_6$)	13.6	0.189	0.011

[a] $1\% = 8.8 \times 10^{19}\ cm^{-3}$ for LiSAF; $9.6 \times 10^{19}\ cm^{-3}$ for LiCAF.

the Mg and Zn codopants cause substantial inhomogeneous broadening of the emission band, as deduced from the emission data in Fig. 4. These spectra were obtained with the 266 nm fourth harmonic of a Nd:YAG laser, and by collecting and processing the Ce emission with a lens system, polarizer, 0.32 m polychromator (150 μm slitwidth; 600 groove mm^{-1} grating), and optical multichannel analyzer (OMA). The increased spectral width of the Mg, Ce:LiSAF crystal indicates that the Mg^{2+} ions impact the nature of the Ce environment, perhaps by substituting for the nearby Al^{3+} ions (for overall charge neutrality). It is noteworthy that the melts containing divalent compensator ions proved more difficult to grow and gave substantially smaller yields. [21].

Part of the motivation for including codopants in the melt is to increase the Ce segregation coefficient, k, defined as Ce^{3+} in the crystal divided by Ce in the melt. From the data in Table 2 it is seen that k is between 0.010 and 0.014 for the pure and Na-doped Ce:LiSAF crystals. This value agrees with our previously assessed [6] constant of $k = 0.013$. It is also noteworthy that the Mg^{2+} and Zn^{2+} codopants actually decrease the Ce^{3+} k-value. Also, Ce:LiCAF offers about half the Ce-content, as previously determined [6].

We explored the solarization behavior of the samples listed in Table 2, and found that the codopants could substantially affect both the shape and strength of the UV-induced spectra. For these experiments, the solarization defects were induced with a 266 nm Nd:YAG pump, while a continuous wave deuterium lamp (filtered through a pinhole) served as the probe source. A polychromator/OMA combination was employed along with lenses and a polarizer to monitor the probe. Importantly, a shutter was also positioned before the polychromator in order to block the (nanosecond timescale) emission light emanating from the sample. The appropriate UV-induced and electronic backgrounds were subtracted from the data using a standard prescription [22] to produce the spectra in Fig. 5.

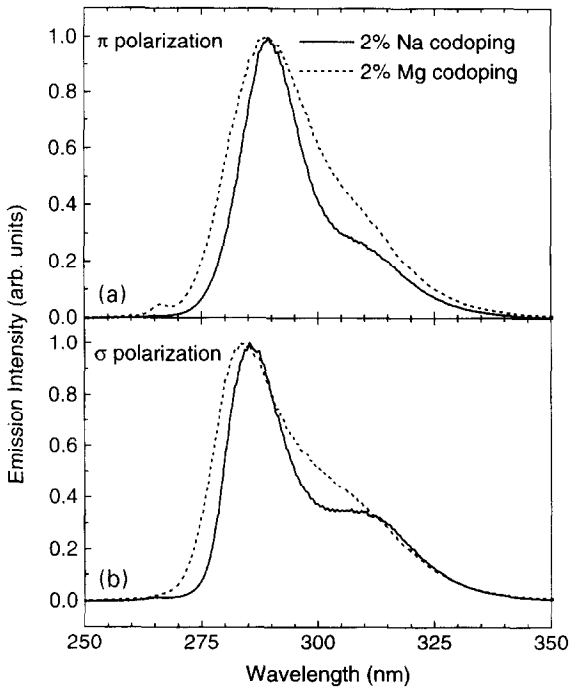

Fig. 4. Comparison of Ce:LiSAF emission spectra obtained with Na^+ and with Mg^{2+} codoping.

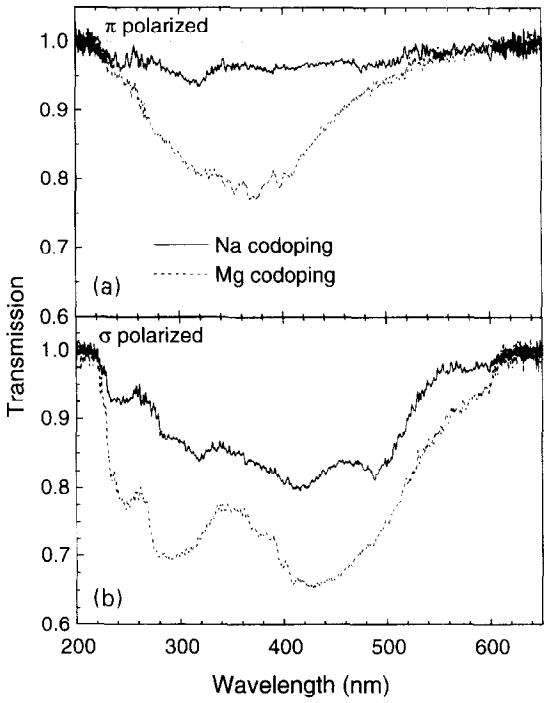

Fig. 5. (a) Solarization spectra of Ce:LiSAF recorded for samples containing Na^+ and Mg^{2+} codopants, employing π-polarized pump and probe light, and (b) with σ-polarized pump and probe light.

Illustrative solarization spectra with the pump and probe beams both π-polarized are shown in Fig. 5(a) for the Na, Ce : LiSAF and Mg, Ce : LiSAF samples. The related fully σ-polarized spectra appear in Fig. 5(b). The Mg-containing material produces a spectrum that is different in shape (possibly broadened), and also considerably stronger for a given pump fluence. In addition, we see that the π-polarized spectra are both weaker and have a different shape than those that are σ-polarized; these differences are beneficial to the π-polarized operation of the laser. Lastly, the very broad spectral width of ~ 2 eV for all the spectra reflect the involvement of the conduction band states as the terminal levels of the electronic transition.

Fig. 6 is a bar chart of the solarization loss levels at 457 nm resulting from the four possible combinations of pump and probe light. Interestingly, the main difference arises from the probe polarization change alone. This observation may seem surprising at first since σ_{ESA} is 4.5× larger in the σ-polarization of the pump beam, leading to a greater solarization rate. As we shall see later, however, a critical ingredient in the solarization mechanism entails the bleaching of the defect by the pump light. Since we also expect the bleaching to be more effective when the laser is σ-polarized (see Fig. 5), we find that the increased color center production is counterbalanced with their increased bleaching, leading to a similar net absorption level. This idea is discussed quantitatively below.

One of the manifestations of bleaching behavior is presented in Fig. 7, which is a logarithmic plot of the defect lifetime, τ_{sol} versus the 457nm intensity, I. The simplest model of light-induced annihilation of the solarization defect population (N_{sol}) can be described with

$$\frac{dN_{sol}}{dt} = \frac{N_{sol} I}{F_0} \tag{3}$$

where F_0 is a fitted constant, and the defect lifetime in the presence of the light field becomes $\tau_{sol} = F_0/I$. Here we assume, and have validated, that the natural lifetime of the defect in the absence of light is very long (≫ days). With the data in Fig. 7 we are able to deduce that $F_0 = 0.7\ J\,cm^{-2}$. On the

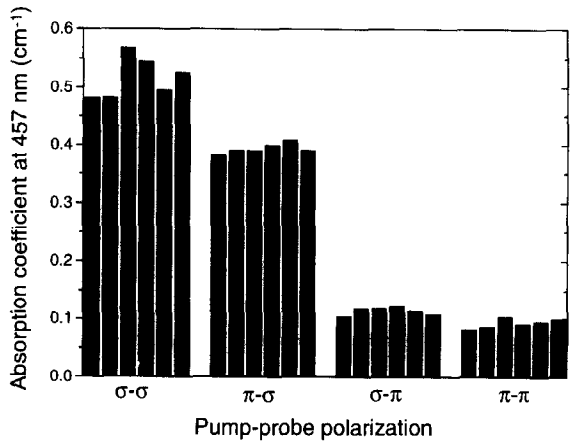

Fig. 6. Comparison of solarization level measured on six different spots for the Ce : LiSAF sample, for each of four possibilities of pump and probe light.

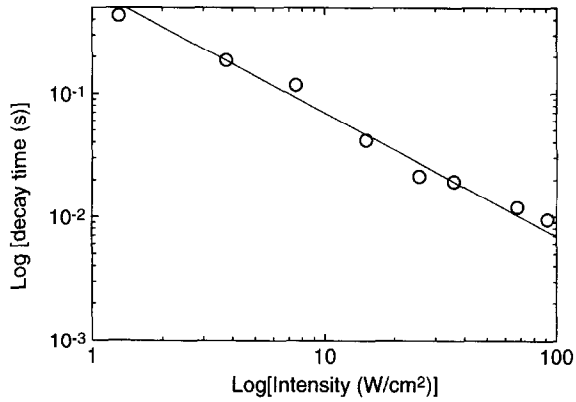

Fig. 7. Plot of the solarization defect lifetime as a function of the intensity of the 457 nm probe beam.

basis of straightforward considerations we can describe F_0 as

$$F_0 = h\nu/(\eta_{bl} \cdot \sigma_{sol}) \tag{4}$$

where σ_{sol} is the defect cross-section and η_{bl} is the efficiency by which the defect can be ionized (i.e. annihilated). From Eq. (4) we calculate that $\eta_{bl}\,\sigma_{sol} = 6.2 \times 10^{-19}\ cm^2$ at 457 nm.

In a separate experiment we examined the saturation of the observed absorption at 457 nm as a function of the 266 nm fluence (Fig. 8) for the case where both beams are σ-polarized. For these

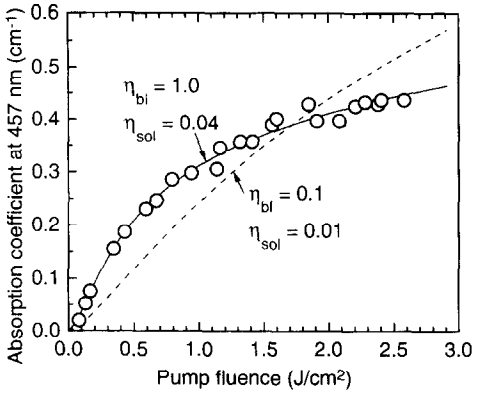

Fig. 8. Observed absorption level at 457 nm induced by varying 266 nm pump fluence.

experiments the 457 nm beam intensity was arranged to be sufficiently intense so that the sample nearly recovered between laser shots at the 10 Hz repetition rate. Using a model based on two-step ionization of the Ce ion with efficiency η_{sol}, followed by bleaching of the defect with efficiency η_{bl} as previously suggested by Hamilton and coworkers [5, 9] we have the population equations:

$$\frac{\partial N_{4f}}{\partial t} = \frac{-\sigma_{abs} N_{4f} I_{266}}{h\nu} + \frac{N_{5d}}{\tau_{5d}}, \tag{5a}$$

$$\frac{\partial N_{5d}}{\partial t} = \frac{+\sigma_{abs} N_{4f} I_{266}}{h\nu} - \frac{N_{5d}}{\tau_{5d}} - \frac{\eta_{sol}\sigma_{ESA} N_{5d} I_{266}}{h\nu} + \frac{\eta_{bl}\sigma_{sol}^{266} N_{sol} I_{266}}{h\nu}, \tag{5b}$$

and

$$\frac{\partial N_{sol}}{\partial t} = \frac{+\eta_{sol}\sigma_{ESA} N_{5d} I_{266}}{h\nu} - \frac{\eta_{bl}\sigma_{sol}^{266} N_{sol} I_{266}}{h\nu}, \tag{5c}$$

and the pump and probe intensities:

$$\frac{\partial I_{266}}{\partial z} = -\sigma_{abs} N_{4f} - \sigma_{ESA} N_{5d} - \sigma_{sol}^{266} N_{sol}, \tag{5d}$$

and

$$\frac{\partial I_{457}}{\partial z} = -\sigma_{sol}^{457} N_{sol} I_{457}. \tag{5e}$$

Here N_{4f}, N_{5d}, and N_{sol} are the populations of the ground and excited states of Ce^{3+}, and that of the solarization defect, respectively. $\tau_{5d} = 28$ ns is the excited state lifetime, I_{266} and I_{457} are the 266 and 457 nm source intensities, respectively. From the fit to Fig. 8 we can derive that $\eta_{bl}\sigma_{sol} = 6.2 \times 10^{-18}$ cm^2 at 266 nm, compared to 6.2×10^{-19} cm^2 from the data in Fig. 7 obtained at 457 nm. Note that the ratio of defect cross-section at 266 and 457 nm is set at $\sigma_{sol}^{266}/\sigma_{sol}^{457} = 0.46$ by the spectral data in Fig. 5(b), so we must conclude that the ratio of the bleaching efficiencies at 457 nm compared to 266 nm is 0.046. While this result could be construed as somewhat surprising, ionization efficiencies are often found to rise with shorter wavelength excitation [15].

Now, upon examining a variety of parameter inputs to the fit of Fig. 8, we find that η_{bl} values of 0.3 to 1.0 are all adequate – we therefore take $\eta_{bl} = 1.0$ at 266 nm somewhat arbitrarily at this point, suggesting that all photons absorbed by the solarization defect lead to its destruction (by liberating its electron into the conduction band.) This assumption implies that $\eta_{bl} = 0.046$ at 457 nm. We were also able to derive the value of the solarization (i.e. formation) efficiency as $\eta_{sol} = 0.039$ at 266 nm, as listed in Table 1.

4. Laser efficiency with antisolarant pump

In order to establish the correlation between the pump-induced solarization and the laser efficiency, it is worthwhile to plot the attained laser slope efficiency (with 50% output coupling) against the actual measured π-polarization loss at 290 nm arising from a 266 nm π-polarized pump beam. To do this several of the slope efficiencies appearing in the first data column of Table 3 are used as the input data points for Fig. 9. The absorbed fraction at 290 nm was determined by employing the same 266 nm pump fluence for each crystal, although the fluence did not correspond to that used in the laser oscillator. In any case, the crucial deduction from Fig. 9 is that the laser slope efficiency has a strong tendency to decrease as the solarization loss rises. Although the experimental errors are substantial

Table 3
Slope efficiencies obtained for Ce:LiSAF laser with and without use of 532 nm antisolarant beam

Crystal sample	Slope efficiency 266 nm pump (%)	Slope efficiency 266 nm pump + 532 nm beam (%)
1.5% Ce:LiSAF	23.9	30.9
2% Ce:LiSAF	16.8	29.6
2% Na, 2% Ce:LiSAF	33.1	46.9
4% Na, 2% Ce:LiSAF	28.8	42.9
2% Mg, 2% Ce:LiSAF	1.1	7.5
2% Zn, 2% Ce:LiSAF	13.0	–
2% Ce:LiCAF	29.0	29.0
2% Ce:Li($Sr_{0.8}Ca_{0.2}AlF_6$)	17.9	27.2

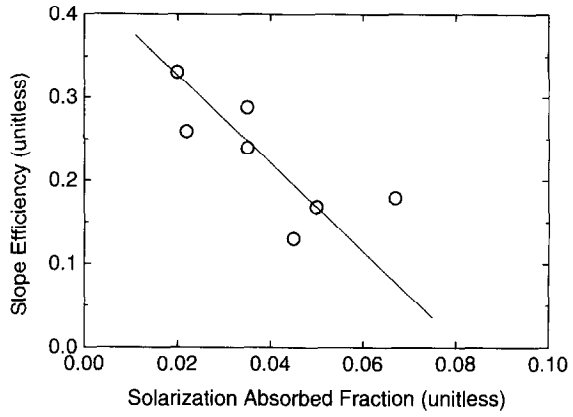

Fig. 9. Plot of the measured slope efficiency of 7 crystals against the absorbed fraction at 290 nm obtained with a 266 nm pump and a deuterium lamp probe.

for the data in Fig. 9, the correlation between decreased efficiency and greater solarization loss is compelling.

Armed with the information that: (a) the solarization losses adversely impact the laser performance, and (b) the solarization loss is bleachable, we may deduce that it is possible to increase the efficiency of the Ce:LiSAF laser by introducing a second antisolarant pump beam. This is most easily accomplished by using the second harmonic of the Nd:YAG pump source at 532 nm.

A clear test of the utility of this approach can be accomplished by operating a π-polarized 266 nm-pumped oscillator along with the additional σ-polarized 532 nm antisolarant beam introduced within the pumped volume. This data appears in Fig. 10, and it can be seen that the laser output energy can be increased from about 0.18 to 0.24 mJ with the 532 nm beam, while keeping the 266 nm energy constant. This data can be fit to the expression:

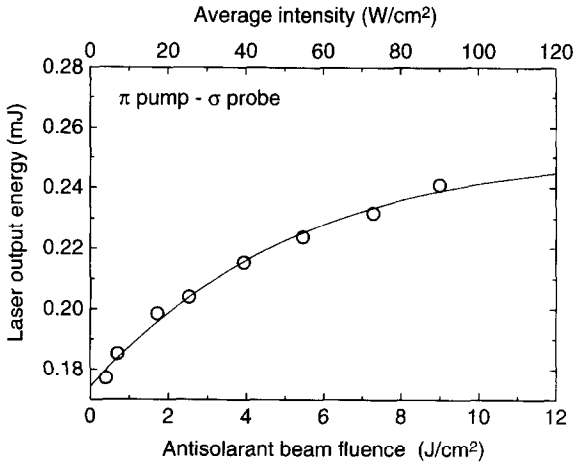

Fig. 10. Graph of 266 nm-pumped Ce:LiSAF oscillator energy as a fraction of the 532 nm antisolarant beam fluence.

$$E_{out} = \eta_0(E_p - E_{th})\left[\frac{\ln(1 - T_{oc})}{\ln(1 - T_{oc}) + \ln[1 - L_{nonbl} - L_{bl}\exp(-F^{532}/F_o^{532})]}\right] \quad (6)$$

where E_{out} is the 290 nm laser output energy, η_0 is the intrinsic efficiency, E_p is the absorbed 266 nm pump energy, E_{th} is the threshold 266 nm pump energy, T_α is the output coupling value, L_{nonbl} and L_{bl} are the double-pass non-bleachable and bleachable portions of the solarization losses, F^{532} is the antisolarant 532 nm pump beam fluence, and F_0^{532} is a fitted constant. The theory curve of Fig. 10 yields $L_{nonbl} = 19\%$, $L_{bl} = 27\%$, and $F_0^{532} = 4.6\ \mathrm{J\,cm^{-2}}$. This F_0 value is roughly consistent with

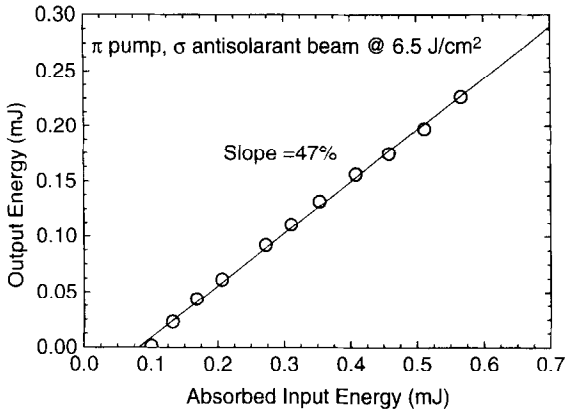

Fig. 11. Slope efficiency plot for 2% Na, 2% Ce:LiSAF laser using a 266 nm pump and a constant 532 antisolarant beam.

the $F_0^{457} = 0.7\,\mathrm{cm}^{-2}$ parameter derived earlier, noting that the spectra of Fig. 5(b) suggest the two values should differ by about a factor of 2.5 (i.e. $4.6\,\mathrm{J\,cm}^{-2}$ measured at 532 nm versus $1.8\,\mathrm{J\,cm}^{-2}$ predicted for 532 nm from the cw 457 nm probe laser experiment). In consideration of the very different natures of the experiments involved in Figs. 7 and 10, it is very encouraging to see that the F_0 constants have similar magnitudes.

We have measured the slope efficiencies of six Ce:LiSAF crystals, some including the Na^+, Mg^{2+} and Zn^{2+} codopants, and have also examined the performance of Ce:LiCAF and of the mixture $Ce:LiSr_{0.8}Ca_{0.2}AlF_6$. Then each of the slope efficiencies was remeasured with the presence of the 532 nm antisolarant beam. In most cases the slope efficiency was significantly enhanced, reaching as high as 47% for the 2% Na, 2% Ce:LiSAF material preparation, as shown in Fig. 11. One notable exception to this phenomenon is the Ce:LiCAF sample, probably because the solarization spectrum is slightly blue-shifted and does not actually overlap the 532 nm antisolarant beam wavelength.

5. Summary

We have attempted to elucidate the mechanism by which UV-induced solarization occurs in Ce^{3+}-doped crystals, paying special attention to its impact on the laser performance of the crystal. While it appears that all Ce^{3+}-doped crystals exhibit some level of solarization, the magnitude of detrimental effect varies greatly – both among different crystalline materials, as well as among varying preparations of a given type of crystal. In the course of this work we have discovered that Na^+ codopants lead to much lower solarization than Mg^{2+} or Zn^{2+} dopants.

We have also found that the solarization defects formed in Ce:LiSAF can be destructively and reversibly bleached with 532 or 457 nm light, which falls within the solarization absorption spectrum, by returning the electron to the conduction band (CB) and therefore back to the cerium ion. Since the color centers are initially formed by way of the $4f \rightarrow 5d \rightarrow CB$ excitation sequence, the creation and annihilation of the color centers reach an equilibrium distribution for each pump level. Interestingly, the remarkably favorable performance of the Ce:LiSAF laser can be traced to either (or both) the reduced creation of color centers or to their enhanced rate of destruction. A detailed model and mathematical fit appear in this article.

Ce:LiSAF has been confirmed to be a robust new laser material, where a slope efficiency of 33% is achievable with a 266 nm pump source, whereas 47% is possible with the introduction of the additional 532 nm bleaching (antisolarant) pump beam. A slope efficiency of 29% was attained for Ce:LiCAF.

Acknowledgements

LLNL personnel performed this work under the auspices of the US Department of Energy, Lawrence Livermore National Laboratory, Contract No. W-7405-ENG-48. Portions of this project were supported by a CRADA (#TSB-950-94), and a Phase I SBIR at LOC funded by the Ballistic Missile Defense Organization – which was monitored and sponsored by the Air Force National Command (#F19629-94-C-0134) at Hanscon Air Force Base.

References

[1] D.J. Ehrlich, P.F. Moulton and R.M. Osgood, Jr., Opt. Lett. 4 (1979) 184.

[2] K.H. Yang and J.A. DeLuca, Appl. Phys. Lett. 29 (1976) 499, ibid. 31 (1977) 594.
[3] D.J. Ehrlich, P.F. Moulton and R.M. Osgood, Jr., Opt. Lett. 5 (1980) 339.
[4] F. Okada, S. Togawa, K. Ohta and S. Koda, J. Appl. Phys. 75 (1994) 49.
[5] G.J. Pogatshnik and D.S. Hamilton, J. Lumin. 38 (1987) 201; G.J. Pogatshnik and D.S. Hamilton, Phys. Rev. B 36 (1987) 8251.
[6] C.D. Marshall, J.A. Speth, S.A. Payne, W.F. Krupke, G.J. Quarles, V. Castillo and B.H.T. Chai, J. Opt. Soc. Am. B 11 (1994) 2054.
[7] M.A. Dubinskii, V.V. Semashko, A.K. Naumov, R.Yu. Abdulsabirov and S.L. Korableva, J. Modern Opt. 40 (1993) 1; ibid. Laser Phys. 3 (1993) 216.
[8] N. Sarukura, Z. Liu, Y. Segawa, K. Edamatsu, Y. Suzuki, T. Itoh, V.V. Semashko, A.K. Naumov, S.L. Korableva, R.Yu. Abdulsabirov and M.S. Dubinskii, Opt. Lett. 20 (1995) 294.
[9] K.-S. Lim and D.S. Hamilton, J. Opt. Soc. Am. B 6 (1989) 1401.
[10] M.A. Dubinskii, V.V. Semashko, A.K. Naumov, R.Yu. Abdulsabirov and S.L. Korableva, Laser Phys. 4 (1994) 480.
[11] D.S. Hamilton, S.K. Gayen, G.J. Pogatshnik, R.D. Ghen and W.J. Miniscalco, Phys. Rev. B 39 (1989) 8807.
[12] J.K. Lawson and S.A. Payne, Phys. Rev. B 47 (1993) 14003.
[13] R.R. Jacobs, W.F. Krupke and M.J. Weber, Appl. Phys. Lett. 33 (1978) 410.
[14] W.J. Miniscalco, J.M. Pellegrino and W.M. Yen, J. Appl. Phys. 49 (1978) 6109.
[15] C. Pedrini, F. Rogemond and D.S. McClure, J. Appl. Phys. 59 (1986) 1196.
[16] J.F. Pinto, G.H. Rosenblatt, L. Esterowitz, V. Castillo and G.J. Quarles, Electron. Lett. 30 (1994) 240.
[17] S.A. Payne, W.F. Krupke, L.K. Smith, W.L. Kway, L.D. DeLoach and J.B. Tassano, IEEE J. Quantum Electron. 28 (1992) 1188.
[18] Cr:LiSAF is available from Lightning Optical Corporation, Tarpon Springs, FL.
[19] P. Rambaldi, M. Douard and J.P. Wolf, Appl. Phys. B 61 (1995) 117.
[20] J.A. Caird, S.A. Payne, P.R. Staver, A.J. Ramponi, L.L. Chase and W.F. Krupke, IEEE J. Quantum Electron. 24 (1988) 1077; S.A. Payne, L.L. Chase, L.K. Smith and B.H.T. Chai, Opt. Quantum Electron. 22 (1990) S259.
[21] V.K. Castillo and G.J. Quarles, in: UV and Visible Lasers and Laser Crystal Growth eds. R. Scheps and M.R. Kokta, Proc. SPIE 2380 (1995) 43–50.
[22] S.A. Payne, L.L. Chase and G.D. Wilke, Phys. Rev. B 37 (1988) 998.